Acta Pharmaceutica Sinica B 2025;15(2):1007−1022

Chinese Pharmaceutical Association
Institute of Materia Medica, Chinese Academy of Medical Sciences

Acta Pharmaceutica Sinica B

www.elsevier.com/locate/apsb
www.sciencedirect.com

ORIGINAL ARTICLE

Extracellular vesicles deliver thioredoxin to rescue stem cells from senescence and intervertebral disc degeneration *via* a feed-forward circuit of the NRF2/AP-1 composite pathway

Xuanzuo Chen[a,†], Sheng Liu[a,†], Huiwen Wang[a,†], Yiran Liu[b], Yan Xiao[c], Kanglu Li[a], Feifei Ni[a], Wei Wu[a], Hui Lin[a], Xiangcheng Qing[a], Feifei Pu[d], Baichuan Wang[a,*], Zengwu Shao[a,*], Yizhong Peng[a,*]

[a]*Department of Orthopaedics, Union Hospital, Tongji Medical College, Huazhong University of Science and Technology, Wuhan 430022, China*
[b]*The First School of Clinical Medicine, Tongji Medical College, Huazhong University of Science and Technology, Wuhan 430022, China*
[c]*Department of Radiology, Union Hospital, Tongji Medical College, Huazhong University of Science and Technology, Wuhan 430022, China*
[d]*Department of Orthopedics, Traditional Chinese and Western Medicine Hospital of Wuhan, Tongji Medical College, Huazhong University of Science and Technology, Wuhan 430022, China*

Received 26 April 2024; received in revised form 1 July 2024; accepted 26 July 2024

KEY WORDS

TXN;
NRF2;
AP-1;
Exosomes;

Abstract Intervertebral disc degeneration (IDD) is largely attributed to impaired endogenous repair. Nucleus pulposus-derived stem cells (NPSCs) senescence leads to endogenous repair failure. Small extracellular vesicles/exosomes derived from mesenchymal stem cells (mExo) have shown great therapeutic potential in IDD, while whether mExo could alleviate NPSCs senescence and its mechanisms remained unknown. We established a compression-induced NPSCs senescence model and rat IDD

*Corresponding authors.
E-mail addresses: pyz5941z@163.com (Baichuan Wang), 1985xh0536@hust.edu.cn (Zengwu Shao), 2012xh0929@hust.edu.cn (Yizhong Peng).
[†]These authors made equal contributions to this work.
Peer review under the responsibility of Chinese Pharmaceutical Association and Institute of Materia Medica, Chinese Academy of Medical Sciences.

https://doi.org/10.1016/j.apsb.2024.12.013

Senescence;
Intervertebral disc degeneration;
NPSCs;
ESCRT

models to evaluate the therapeutic efficiency of mExo and investigate the mechanisms. We found that mExo significantly alleviated NPSCs senescence and promoted disc regeneration while knocking down thioredoxin (TXN) impaired the protective effects of mExo. TXN was bound to various endosomal sorting complex required for transport (ESCRT) proteins. Autocrine motility factor receptor (AMFR) mediated TXN K63 ubiquitination to promote the binding of TXN on ESCRT proteins and sorting of TXN into mExo. Knocking down exosomal TXN inhibited the transcriptional activity of nuclear factor erythroid 2-related factor 2 (NRF2) and activator protein 1 (AP-1). NRF2 and AP-1 inhibition reduced endogenous TXN production that was promoted by exosomal TXN. Inhibition of NRF2 *in vivo* diminished the anti-senescence and regenerative effects of mExo. Conclusively, AMFR-mediated TXN ubiquitination promoted the sorting of TXN into mExo, allowing exosomal TXN to promote endogenous TXN production in NPSCs *via* TXN/NRF2/AP-1 feed-forward circuit to alleviate NPSCs senescence and disc degeneration.

1. Introduction

Low back pain (LBP), a leading cause of disability, has a point prevalence of 11.9% (standard deviation (SD) 2%) and one-month prevalence of 23.3% (SD 2.9%) and was most common in middle-aged to older women (*i.e.*, 40−80 years) based on a review of 165 studies from 54 countries[1]. LBP seriously affects the quality of life of patients and causes a heavy medical and financial burden to society. Roughly 70%−80% of patients with intervertebral disc degeneration (IDD) experience low back pain in their lifetime[2]. Approximately 40% of chronic LBP cases were attributed to the symptomatic IDD[3]. At present, the therapeutic outcome of clinical treatment methods (drugs, physiotherapy, surgery, etc.) mostly alleviates symptoms, but cannot inhibit the progress of IDD, and the therapeutic outcome is not always satisfying[4].

Stem-cell-based therapies have shown great potential in IDD therapy. Nucleus pulposus stem cells (NPSCs) are the endogenous stem cells resident in disc tissue, which can differentiate into nucleus pulposus cells after mobilization[5]. Compared with mature nucleus pulposus cells, they have higher proliferative activity and deeply participate in the endogenous repair process of intervertebral discs[6,7]. However, the harsh microenvironment in degenerated discs, including the excessive loading, impairs the restorative function of NPSCs and increases cell death, thereby leading to the occurrence and development of IDD[5]. Strategies to intervene in the death of NPSCs had achieved partial inhibition of intervertebral disc degeneration[5,8]. However, since the endogenous repair capacity of survived NPSCs in the degenerative tissue is impaired, it is difficult to achieve satisfactory results by solely interfering with the death of NPSCs. It is also necessary to restore the function of NPSCs to jointly promote the endogenous repair of intervertebral disc[9,10].

Cellular senescence plays a critical role in cell dysfunction, which is manifested by the cycle block, the decline of proliferation, and differentiation ability[11], thereby significantly weakening the potential of NPSCs for tissue regeneration[12,13]. Moreover, the senescent cells also aggravate the inflammatory microenvironment through the secretion of senescence-associated secretory phenotype (SASP) that further induces the senescence of surrounding cells, which deeply participates in the degeneration and progress of intervertebral discs[10,14]. Exosomes derived from mesenchymal stem cells (mExo) are characterized by stable nature, easy preservation, and low immunogenicity[15−17]. mExo has shown the capacity to alleviate cell death and dysfunction of nucleus pulposus cells and has broad prospects in the field of IDD treatment[18]. However, the underlying mechanism of mExo on alleviating the senescence of NPSCs has not been clarified.

In this study, we established compression-induced NPSCs senescence and rat IDD model and investigated the protective effects of small extracellular vesicles derived from mesenchymal stem cells (MSC). Then, we screened the protein composition of mExo based on EVpedia and the GSEA database and identified a key regulator, thioredoxin (TXN), that mediated the regenerative effects of mExo against cellular senescence and disc degeneration. Furthermore, the underlying mechanisms of TXN sorting into mExo and how exosomal TXN performed anti-senescence effects were carefully clarified. Notably, our results demonstrated that after Autocrine motility factor receptor (AMFR) ubiquitination modification, TXN is presented to NPSCs from mExo *via* the Endosomal Sorting Complex Required for Transport (ESCRT) pathway, and formed a feed-forward circuit of the nuclear factor erythroid 2-related factor 2 (NRF2)-activator protein 1 (AP-1) composite pathway to establish an anti-oxidative pattern, thus, delaying the senescence of NPSCs and inhibiting intervertebral disc degeneration.

2. Materials and methods

2.1. Nucleus pulposus stem cells (NPSCs) culture and characterization

All the procedures were approved by the Medical Ethics Committee of Tongji Medical College, Huazhong University of Science and Technology, Wuhan, China. Intervertebral disc specimens were collected with informed consent from patients. Briefly, the nucleus pulposus tissue of the intervertebral disc above, 1/2 mass of which was reserved for subsequent testing, and the remaining tissue was cut into pieces with sterile conditions and digested with 0.25% type II collagenase (Sigma, St. Louis, MO, USA) at 37 °C for 6 h. Centrifuged at 300×*g* for 5 min and discarded, the supernatant was resuspended with human mesenchymal stem cell medium (Cyagen, San Francisco, USA) and transferred to a T25 culture flask for culture (37 °C, 5% CO_2). The

medium was changed every 3 days and passed after the confluence reached 80%−90%. NPSCs were cultured in different sequential media using osteogenic, chondrogenic, and adipogenic differentiation kits (Corning, New York, NY, USA). Alizarin Red, Oil Red, and Alcian Blue (Leagene Biotechnology, China) were used to detect the multipotential differentiation capabilities of NPSCs (Supporting Information Fig. S1). Recombinant TXN was purchased from MedChemExpress (New Jersey, USA) for the experimental treatment of NPSCs.

2.2. Bone marrow mesenchymal stem cells (BMSCs) culture and characterization

Bone marrow samples were obtained from patients undergoing artificial hip joint replacements. We collected 10 mL of human bone marrow blood samples and quickly transferred them to sterile tubes for centrifugation at 300 × *g* for 5 min. The supernatant was discarded, washed twice with phosphate-buffered saline (PBS), resuspended in human mesenchymal stem cell culture medium (Cyagen), and inoculated in a T25 culture flask (37 °C, 5% CO_2) for culture. After 24 h, half of the medium was changed. After 48 h, the flask wall was gently washed with preheated PBS. Next, the medium was changed every 2−3 days. The cells were digested with ethylenediaminetetraacetic acid (EDTA)−trypsin and passaged when growing in a vortex shape. As above, the differentiation ability of BMSCs was evaluated by three-lineage differentiation kits (Fig. S1).

2.3. Isolation and characterization of mExo

The second-generation BMSCs were seeded in T75 culture flasks and cultured in 37 °C, 5% CO_2. After reaching 90% confluence, serum-free DMEM/F12 was added, and after 48 h, the cell supernatant was collected to extract mExo by differential centrifugation. In short, the medium was centrifuged at 300 × *g* for 10 min, then 2000 × *g* for 30 min. Next, the supernatant was collected and centrifuged at 10,000 × *g* for 30 min, then the harvested supernatant was filtered through a 0.22 μm filter (Millipore, Massachusetts, USA) and centrifuged by ultracentrifugation at 100,000 × *g* (Beckman Type 70 Ti, California, USA) for 70 min. A bicinchoninic acid protein assay kit (Boster, China) was adopted to measure the concentration of mExo, and the pellet was collected, suspended in 50 μL PBS, and stored at −80 °C.

The NanoSight NS300 system (Malvern, UK) was applied to measure the particle size of mExo and the structure of mExo was observed by transmission electron microscopy. Western Blot detects the mExo surface marker proteins, including TSG101 (ABclonal, A2216, China), CD63 (Abcam, ab271286, UK), CD9 (Abcam, ab263019, UK), and calnexin (Abcam, ab92573, UK).

2.4. Senescence-associated β-galactosidase (SA-β-gal) staining

The SA-β-gal staining kit (Beyotime Biotechnology, China) was used to evaluate the characteristics of cellular senescence. According to the manufacturer's protocol, cells were firstly fixed with 4% paraformaldehyde for 30 min and washed with PBS three times, then the mixed x-gal staining solution was added into samples and incubated overnight. An optical microscope (Olympus, Japan) was used to capture pictures, and ImageJ was used to calculate the number of SA-β-gal-positive cells.

2.5. Analysis of cell cycle by flow cytometry

The culture medium was removed and cells were washed with PBS three times. Then, 1×10^6 cells were harvested in pre-iced 70% ethanol solution and placed at 4 °C for 2 h, then cells were centrifuged at 300 × *g* for 5 min to decant ethanol completely. Cell pellets were washed with pre-cool PBS three times and suspended in 200 μL of propidium iodide (PI) staining solution (0.1% (*v*/*v*) Triton X-100, 10 μg/mL PI (Molecular Probes, Inc., China), and 100 μg/mL DNase-free RNase A in PBS), and incubated in dark at 25 °C for 30 min. Flow cytometer (BD LSR II; Becton Dickinson, NJ, USA) and ModFit LT 5.0 were used to analyze the FCS data.

2.6. IDD model establishment and mExo injection

The IDD model establishment procedure was carried out as previously described, with the ethical approval of the Institutional Animal Care and Use Committee, Huazhong University of Science and Technology. SD male rats were anesthetized with 0.6% (*w*/*v*) pentobarbital (40 mg/kg), and the coccygeal vertebrae Co5/6 were located by manual palpation. We then used a 20-G sterile needle to puncture the intervertebral disc at a depth of 5 mm, rotated the needle, and held it for 30 s mExo and NRF2 short hairpin RNA (shRNA) virus (*shNRF2*) injection was carried out every week *via* microsyringes (Hamilton, Switzerland) attached to 29-G needles. The first batch of rats was randomly divided into four groups: Intact, IDD, mExo-50, and mExo-100. The intact group received no operation. IDD group was injected with 2 μL normal saline. mExo-50, and mExo-100 groups were injected with 2 μL mExo (50 μg/mL) and mExo (100 μg/mL), respectively. The second batch of rats were randomly divided into six groups: Intact, IDD, IDD + $mExo^{NC}$, IDD + $mExo^{NC}$ + *NC*, IDD + $mExo^{shTXN}$, IDD + $mExo^{NC}$ + *shNRF2*. IDD + mExo groups were injected with 2 μL mExo (100 μg/mL). IDD + $mExo^{shTXN}$ groups were injected with 2 μL $mExo^{shTXN}$ (100 μg/mL). IDD + $mExo^{NC}$ + *NC* groups were injected with 2 μL solution containing $mExo^{NC}$ (100 μg/mL) and negative control vehicle (6.67×10^9 virus particles/mL). IDD + $mExo^{NC}$ + *shNRF2* were injected with a 2 μL solution containing $mExo^{NC}$ (100 μg/mL) and *shNRF2* (6.67×10^9 virus particles/mL). After 4 weeks, radiography and histological analyses were performed to evaluate the degeneration of intervertebral discs.

2.7. Magnetic resonance imaging (MRI) analysis

The T2-weighted midsagittal sections of the spine were pictured *via* a 3.0-T MRI scanner (GE Medical Systems, UK), and three radiologists evaluated the discs independently referring to the Pfirrmann MRI-grade system. T20-weighted signaling intensity was analyzed by ImageJ (National Institutes of Health, MA, USA). The hydration of disc tissues was calculated by Eq. (1):

$$\text{Relative water content} = \frac{D_s}{D_0} \quad (1)$$

where D_s is T2-weighted intensity of discs after surgery, and D_o is T2-weighted intensity of intact discs.

2.8. Disc height measurement

The rats were anesthetized and radiographed using an X-ray system (Bruker MS FX Pro). Radiographs were obtained using an

exposure time of 30 s and a penetration power of 35 kV. X-ray photographs were then quantified using the intervertebral disc height index (DHI) according to the previous study[19].

2.9. Histopathological and immunochemical evaluation

Rat disc tissues were fixed in paraformaldehyde (4%, *w/v*) and decalcified. After embedding in paraffin, discs were cut into 4.0 μm sections *via* a rotary microtome (Thermo Fisher Scientific, MA, USA). Next, slides were stained with hematoxylin−eosin (HE) staining and safranin O-fast green (SO) staining. Histological grading was carried out independently by three pathologists according to the histological grading scale of Han et al.

Immunohistochemical staining with primary antibodies against p16 (ABclonal, A0262, China) and p21 (ABclonal, A11454, China) was performed. Five fields of vision for each slide were randomly adopted under high magnification *via* an optical microscope (Olympus, Tokyo, Japan) for quantitative analysis and the proportion of positively stained cells was calculated.

For immunofluorescence analysis, cells were fixed and incubated with primary antibodies against p16 (ABclonal, A0262, China), p21 (ABclonal, A11454, China), and TEK/TIE2 (Santa Cruz, sc-518137, USA). Fluorescence-conjugated secondary antibodies (Invitrogen, USA) were used to detect fluorescent signals before adding 4′,6-diamidino-2-phenylindole (DAPI, Sigma). An anti-fluorescence quenching sealer (ThermoFisher Scientific) was dropped onto the cell slides and a fluorescence microscope (Olympus, Tokyo, Japan) was used to visually sample fluorescence signals.

2.10. Western blot

The culture medium was removed and cells were washed and harvested in lysis buffer (Beyotime) added with the protease inhibitor phenylmethanesulfonylfluoride (PMSF, Beyotime) and phosphatase inhibitor cocktail I (Sigma). An ultrasonic cell disruptor (Sonics & Materials, Inc., USA) was used to sonicate cell lysates and then the cell lysates were centrifuged at 1500 × *g* for 15 min. Supernatants were harvested and the concentration of protein was tested *via* a bicinchoninic acid (BCA) protein assay kit (Boster, China). Next, the supernatants were denatured using a sodium dodecyl sulfate-polyacrylamide gel electrophoresis (SDS-PAGE) denaturation buffer (Servicebio, China). Proteins were transferred from gels onto polyvinylidene fluoride (PVDF) membranes and blocked. The primary antibodies were p16 (ABclonal, A0262, China), p21 (ABclonal, A11454, China), TXN (ABclonal, A4024, China), RPS27A (ABclonal, A2027, China), MAPK1 (ABclonal, AP0472, China), Alix (ABclonal, A2215, China), VPS28 (ABclonal, A9104, China), VPS4A (ABclonal, A7096, China), CHMP4B (ABclonal, A7402, China), CHMP1B (ABclonal, A8239, China), HGS (ABclonal, A1790, China), STAM (ABclonal, A4198, China), TSG101/VPS23 (ABclonal, A2216, China), NQO1 (ABclonal, A19586, China), SOD1 (ABclonal A0274, China), Catalase (ABclonal, A11780, China), GAPDH (ABclonal, AC001, China). Membranes were immunoblotted overnight at 4 °C and were then incubated with secondary antibodies for 1 h at around 24 °C. The protein bands were visualized using enhanced chemiluminescence (Bio-Rad, CA, USA) and data were managed using ImageJ and GraphPad Prism 8.

2.11. Plasmids transfection

The entire human TXN coding region or its mutant was cloned in a *pcDNA3.1+-Amp-Myc* plasmid. The entire human AMFR coding region or its mutant was cloned in *pcDNA3.1+-Amp-Flag* plasmid. The plasmids were extracted following the instructions of EndoFree Mini Plasmid Kit (Tiangen Biotech, China), and transfected into HEK 293T cells with Lipofectamine 3000 (Thermo Fisher Scientific). Briefly, 2 μL Lipofectamine 3000 was added into 125 μL opti-MEM mixture containing 2 μg plasmid and 2 μL P300 reagent. After mixing gently and incubating for 15 min at around 24 °C, the mixture was added to cells at 60%−70% cell confluence. The transfection medium was changed with a complete culture medium after 24 h. After culturing for another 48 h, cells were harvested for further experiments.

2.12. Co-immunoprecipitation (Co-IP) assay

The cell lysates treated with immunoprecipitation lysis buffer were incubated with anti-MYC antibodies or IgG for 2 h at 4 °C with shaking. The immune complex solution was incubated with protein A/G magnetic beads (ABclonal, China) overnight at 4 °C and then washed to remove the unbound immune complex. The immune complex was dissociated from the beads with SDS-PAGE denaturation buffer for Western blot analysis. The primary antibodies used in Co-IP were anti-TXN (ABclonal, A7638, China), anti-HA (ABclonal, AE008, China), anti-MYC (ABclonal, AE070, China), and DDDK-Flag (ABclonal, AE092, China). Secondary antibodies were anti-mouse IgG heavy chain (ABclonal, AS064, China), anti-rabbit IgG heavy chain (ABclonal, AS063, China), and anti-rabbit IgG light chain (ABclonal, AS061, China).

2.13. Lentiviral infection

TXN shRNA (*shTXN*), AMFR shRNA (*shAMFR*), and mCherry-TXN overexpression lentiviral vectors containing puromycin resistance sites were designed and constructed (Shanghai Genechem Co., Ltd., Shanghai, China). After transfecting 293T cells with lentiviral plasmids using transient lipofectamine-mediated cotransfection, the culture supernatants containing lentiviral particles were collected. After concentration and purification, the titers of lentiviral particles were determined. BMSCs or NPSCs were incubated with the respective viruses, while negative control (NC) shRNA lentivirus infection on these cells was used as control groups. Infected cells were selected with a cell culture medium containing 1.5 μg/mL puromycin (Sigma−Aldrich, MO, USA) for one week before experiments were performed. Reverse transcription (RT)-quantitative polymerase chain reaction (qPCR) and Western blot were carried out to evaluate the efficiency of gene knockdown or overexpression.

2.14. Chromatin immunoprecipitation(ChIP)-qPCR assay

According to the manufacturer's protocol of Enzymatic Chromatin IP Kit (9003, CST, USA), cells were collected and centrifuged after fixation with a final concentration of 1% formaldehyde. The supernatant was removed from the samples, and the pellets were subjected to nuclear processing and chromatin shearing to produce appropriate DNA fragments. The fragments were immunoprecipitated with NRF2 (ab62352, Abcam, MA, USA). The chromosomes were eluted from the protein G microspheres and de-crosslinked. The DNA samples were purified and collected for qPCR assay. Gene expression

was detected *via* the SYBR PrimeScript RT-PCR Kit (Vazyme Biotech Co., Ltd., China) on the Step One Plus Real-Time PCR system (Bio-Rad, Hercules, CA, USA). The results were presented as a percentage of the input. The primers for ChIP-qPCR are listed in Supporting Information Table S1.

2.15. RNA sequencing and bioinformatic analysis

After treatment, total RNA was extracted using the TRIzol Reagent according to the manufacturer's instructions. After RNA quality control, the cDNA sequencing libraries were prepared for next-generation sequencing (NGS) using NGS Library Preparation Kits. Raw reads were preprocessed using fastp v.0.22.0 and mapped against the human reference genome (GRCh38) using STAR v2.7.10b. The expression level of each gene was calculated using featureCounts. Then, differential expression analysis was performed using the R package DEseq2 and R v4.2.2. Several cellular senescence-related gene sets were downloaded from MSigDB v7.5.1 and used to perform Gene set enrichment analysis (GSEA) on the fold change-ranked gene list by the R package clusterProfiler. An algorithm named Virtual Inference of Protein-activity by Enriched Regulon analysis (VIPER) diagram was performed to predict activities of transcription factors from the gene expression of their targets using the R package DoRothEA[20]. Data on the transcription factor regulon networks was downloaded from OmniPath, which is a database of molecular biology prior knowledge.

2.16. AP-1 binding assay

According to the manufacturer's protocol of the TransAM AP-1 family kit (Active Motif, 44296), cells were treated and collected and the cell nuclear extracts were obtained using the Nuclear Extract Kit. Then the cell nuclear extracts were treated with a complete binding buffer and complete lysis solution, and AP-1 antibodies (c-JUN, c-FOS, and JUNB) were added and incubated for 1 h at room temperature. The HRP-labeled secondary antibody was added for incubating for 1 h. Each experimental well was added with 100 μL of chromogenic reagent and then incubated at room temperature for 20 min. During this period, observe the color changes of the sample wells to be tested and the positive control wells, when the color changes from medium blue to dark blue. The absorbance was then measured using a spectrophotometer at an optical density value of 450 nm.

2.17. Statistical analyses

The data are presented as the mean ± standard deviation (SD) from at least three independent experiments and were analyzed *via* SPSS statistical software (IBM Corporation, New York, NY, USA). Student's *t*-test was used for comparisons in GraphPad Prism 7 software (GraphPad Software Inc., CA, USA). All statistical charts were drawn using the GraphPad Prism 7 software. P values < 0.05 were considered statistically significant in all tests.

3. Results

3.1. mExo alleviates compression-induced NPSC senescence

Human NPSCs were cultured under 1.0 MPa compression for 0, 24, and 36 h before SA-β-gal staining, cell cycle flow cytometry, and Western blot detection. SA-β-gal staining showed that the rate of SA-β-gal positive cells increased with the prolongation of compression time (Supporting Information Fig. S2A). Cell cycle flow cytometry indicated that the cell cycle was blocked in the G1/S phase, and the G2/M phase was significantly shortened after compression for 36 h (Fig. S2B). The expression of p16 and p21 proteins was increased after 36 h compression (Fig. S2C). Therefore, 1.0 MPa compression for 36 h significantly induced the senescence phenotype of NPSCs.

mExo were collected from the culture medium of BMSCs. Scanning electron microscopy showed that the vesicles have a typical membranous structure (Fig. 1A). Nanoparticle tracking analysis showed that the mean size of vesicles was around 105 nm, which fits the definition of small extracellular vesicles (50−200 nm)[21] (Fig. 1B). Positive markers (CD63, TSG101, and CD9) and negative markers (calnexin) of mExo were evaluated to identify their characteristics (Fig. 1C). NPSCs were treated with mExo (50 and 100 μg/mL) for 24 h and 1.0 MPa compression for another 36 h. SA-β-gal staining showed that 100 μg/mL mExo significantly reduced the positive staining rate (Fig. 1D and E). The upregulation of p16, p21, and p53 expression induced by compression was reduced by 100 μg/mL mExo (Fig. 1F). Besides, Flow cytometry showed that 100 μg/mL mExo increased the proportion of cells in the G2/M phase and relieved the cycle arrest caused by compression (Fig. 1G). Therefore, mExo effectively delayed NPSCs senescence.

3.2. mExo alleviate intervertebral disc degeneration and tissue senescence

A rat IDD model was established to assess the regenerative effects of mExo; 4 weeks after the first dose of mExo for disc injection, MRI showed that mExo maintained the water content of NP tissue and reduced the degenerative degree of IVD, according to the Pfirrmann grading system (Fig. 2A−C). Besides, mExo maintained the disc height, according to the DHI drawn from the X-ray images (Fig. 2D and E). In the IDD group, NP tissues were shrunken and irregularly shaped, and AF tissues were inward bulging and ruptured, with severe interruption of the border between NP and AF tissues. mExo injection significantly alleviated morphological aggravation and reduced the degenerative histological scoring (Fig. 2F and G). Immunofluorescence of NPSCs biomarker (TEK/TIE2)[22] and senescence-related proteins showed that mExo significantly reduced the expression of p16 and p21 positive cells in TEK^+ cells (Fig. 2H and Supporting Information Fig. S3). Besides, immunohistochemical staining of p16 and p21 suggested that mExo reduced the number of cells positively stained with senescence-related proteins (Supporting Information Fig. S4).

3.3. TXN mediated protective effects of mExo against NPSCs senescence

Based on the EVpedia extracellular vesicle proteomics database and aging genes sets in the GSEA database, we conducted intersection analysis and found that three aging-related proteins including TXN, Ribosomal protein S27a (RPS27A), and mitogen-activated protein kinase 1 (MAPK1), were highly expressed in mExo (Fig. 3A). Among them, TXN, a small mercaptan oxidoreductase, has been reported to alleviate the DNA damage of hematopoietic stem cells caused by radiation, thus delaying cell senescence[23,24]. Compression significantly downregulated TXN, but not RPS27A nor MAPK1 (Fig. 3B and C). We found that *shTXN* lentivirus transfection into BMSCs reduced the protein content of TXN in mExo (Supporting Information Fig. S5).

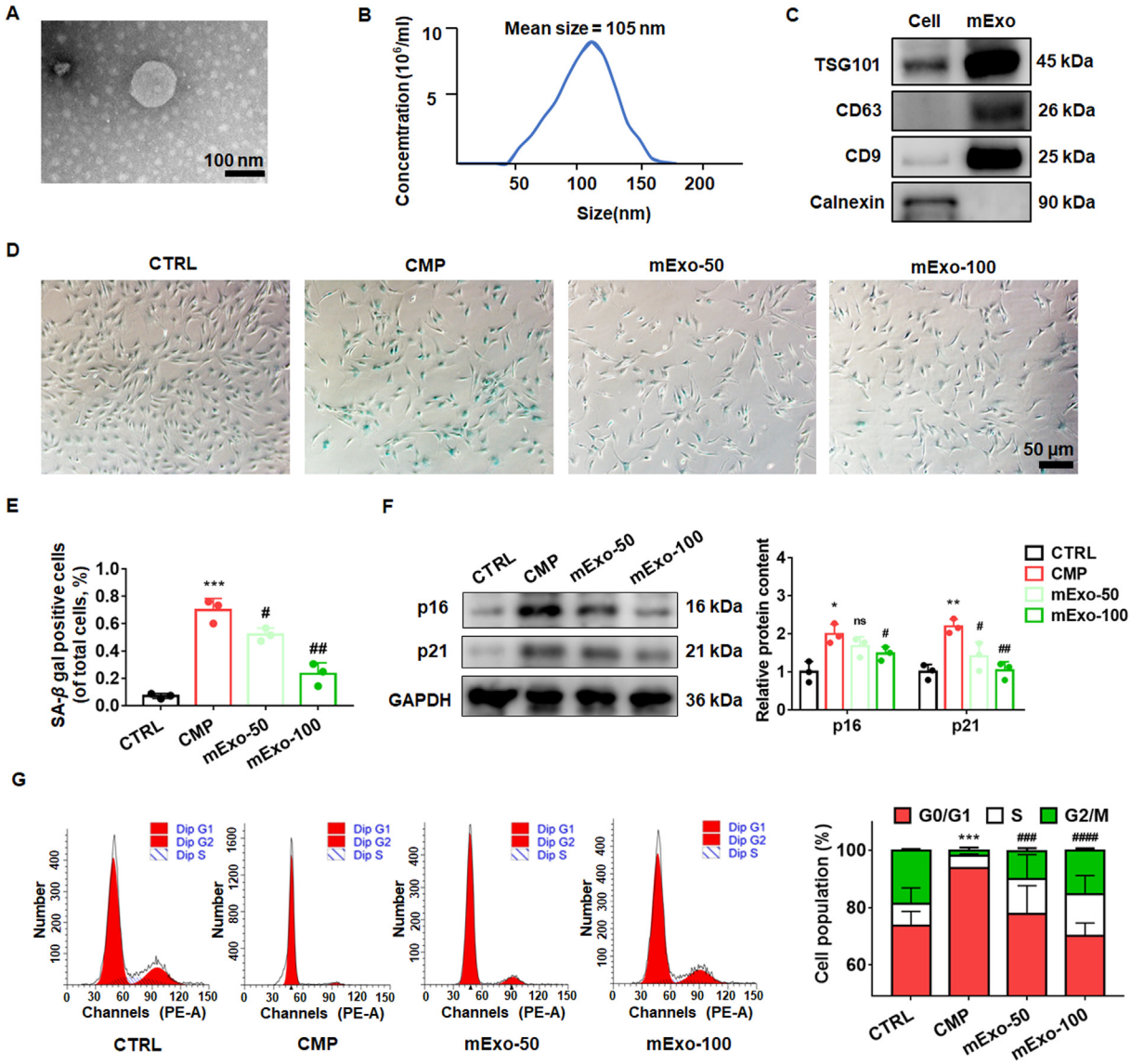

Figure 1 mExo alleviated compression-induced NPSCs senescence. (A) Morphology of vesicles was detected by scanning electron microscope. Scale bar, 100 nm. (B) Isolated mExo was examined by nanoparticle tracking analysis. (C) Protein markers of mExo were assessed by Western blot. (D) NPSCs were evaluated by SA-β-gal staining, and positive staining cell percentages were quantitatively analyzed. Scale bar, 50 μm. (E) Quantitative analysis of positive staining cell percentages. (F) Western blot showed the changes in p16 and p21 expression. Densitometric analysis indicated the fold change of senescence-related proteins. Densitometric analysis was normalized to the CTRL group. (G) Flow cytometry showed cell distribution in the G0/G1, S, and G2/M phases. Data are presented as the mean ± SD, $n = 3$. $^{*}P < 0.05$, $^{**}P < 0.01$, $^{***}P < 0.001$ between CTRL and CMP groups. ns, no significance, $^{\#}P < 0.05$, $^{\#\#}P < 0.01$, $^{\#\#\#}P < 0.001$, $^{\#\#\#\#}P < 0.0001$ between CMP and other groups.

Compared with cells treated with mExo derived from BMSCs with negative control lentivirus infection (mExo^{NC}), the NPSCs in the mExo^{shTXN} group showed increased SA-β-gal positive staining rate (Fig. 3D and E), elevated content of p16 and p21 protein (Fig. 3F), and decreased proportion of G2/M cells (Fig. 3G). These results suggest that mExo alleviated NPSCs senescence by presenting TXN.

3.4. E3 ubiquitin ligase, AMFR, mediates the sorting of TXN into mExo via ESCRT pathway

Mass spectrometry analysis of immunoprecipitation using TXN primary anti-body indicated that TXN combined with various ESCRT proteins (Fig. 4A and B), which suggests that TXN was sorting into mExo through the ESCRT pathway. Supportively, the Co-IP assay confirmed the binding of TXN with ESCRTs including ESCRT-0 (HGS, STAM), ESCRT-I (TSG101, VPS28), and ESCRT-III (VPS4A, CHMP1B) (Fig. 4C). Ubiquitination is a critical pre-requisite for protein sorting mediated by ESCRT pathway[25]. We found that TXN also interacts with E3 ligase AMFR (Fig. 4C). After knocking down the AMFR in BMSCs, the overall level of TXN did not change significantly, while TXN polyubiquitination decreased significantly, especially K63-linked polyubiquitination (Fig. 4D). AMFR knockdown also reduced the affinity of TXN to ESCRTs (Fig. 4E). Moreover, the protein content of TXN in the mExo decreased after silencing AMFR in BMSCs (Fig. 4F). Therefore, the

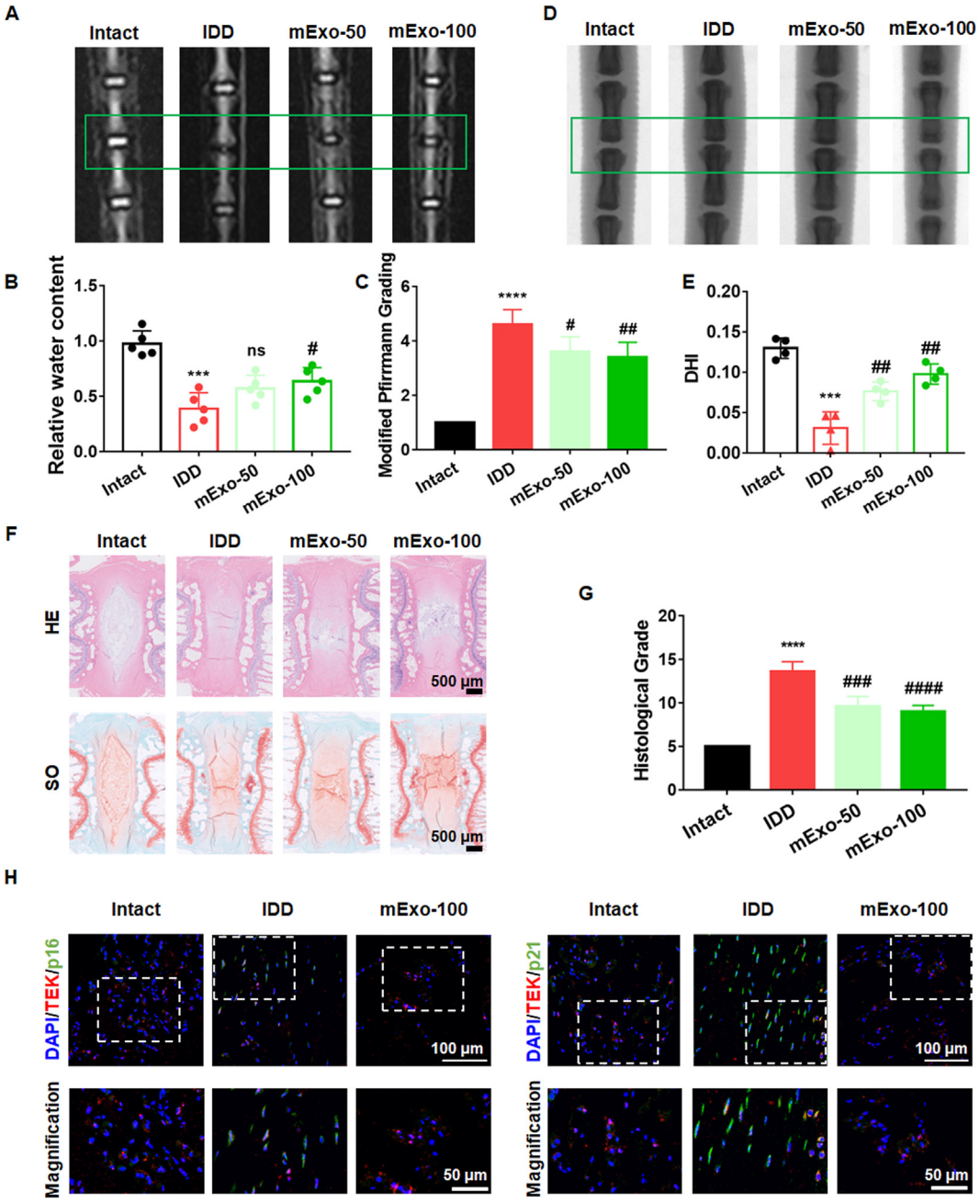

Figure 2 mExo alleviated the degeneration and senescence of intervertebral disc tissue. (A) Representative T2-weighted MRI images of rat tail after mExo intradiscal injection. Green box indicates the operated discs. (B) Relative water content of disc tissue (T2-phase signal of operated NP tissue/T2-phase signal of adjacent NP tissue). (C) Modified Pfirrmann grading based on T2-weighted MRI images. (D) Representative radiographs of rat tail after mExo intradiscal injection. Green box indicates the operated discs. (E) Quantitative analysis of radiographs based on the DHI index. (F) Hematoxylin−eosin staining and safranin O-fast green staining of operated discs. Scale bar, 500 μm. (G) Histological grading scale based on Han et al.[19]. (H) Immunofluorescence images of p16 and p21 expression in TEK^+ cells. Scale bar, 50 and 100 μm. Data are presented as the mean ± SD, $n = 5$. $^{***}P < 0.001$, $^{****}P < 0.0001$ between Intact and IDD groups, $^{\#}P < 0.05$, $^{\#\#}P < 0.01$, $^{\#\#\#}P < 0.001$, $^{\#\#\#\#}P < 0.0001$ between IDD and other groups. ns, no significance. IDD, intervertebral disc degeneration. mExo, exosomes derived from bone mesenchymal stem cells. DHI, disc height index.

ubiquitination modification of TXN mediated by AMFR promotes the sorting of TXN into the mExo.

To further verify the AMFR-mediated TXN ubiquitination, we transfected 293T cells with MYC-tagged TXN, HA-tagged ubiquitin, and Flag-tagged AMFR expression plasmids. We found that TXN was significantly polyubiquitinated by AMFR, and the truncated mutant of AMFR, AMFR-ΔRING, failed to increase the ubiquitination of TXN (Fig. 5A and B). Then, HA-tagged mutant ubiquitin (K48R or K63R), in which the K48 or K63 lysine residue is substituted with arginine, was applied to evaluate the type of polyubiquitination mediated by AMFR on TXN. The polyubiquitination of TXN by AMFR was downregulated in the

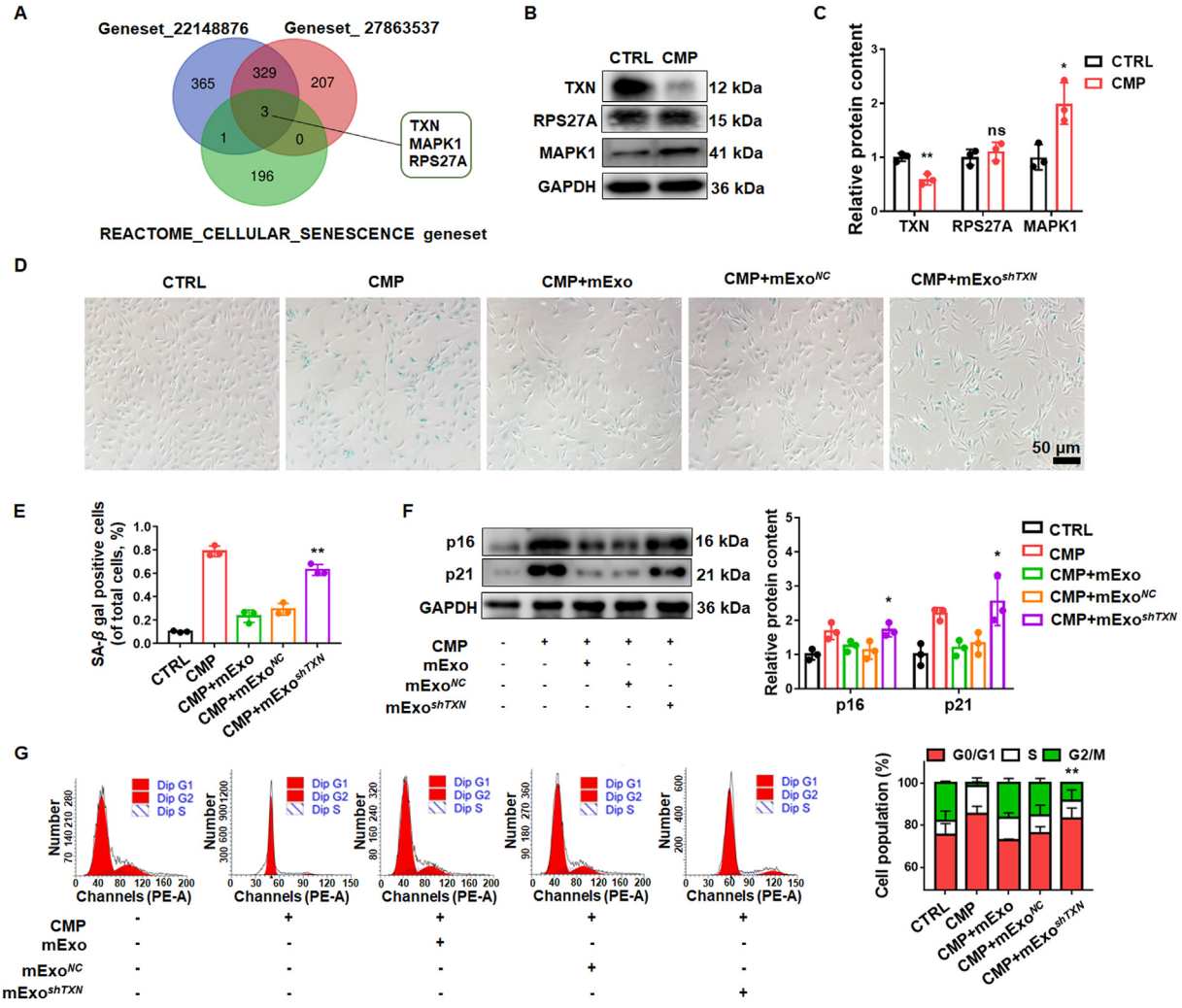

Figure 3 mExo-mediated NPSCs senescence alleviation was regulated by TXN. (A) Venn diagram screening key proteins based on the EVpedia proteomics database and GSEA database. (B) Western blot analysis of screened proteins (TXN, RPS27A, and MAPK1). (C) The densitometric analysis of TXN, RPS27A, and MAPK1 expression in NPSCs. (D) SA-β-gal staining of NPSCs treated with compression and mExo. Scale bar, 50 μm. (E) Quantitative analysis of positive staining cell percentages. (F) Western blot and densitometric analysis of p16 and p21 expression in NPSCs with different treatments. Densitometric analysis was normalized to the CTRL group. (G) Flow cytometry showing the distribution of the cells in G0/G1, S, and G2/M phases. Data are presented as the mean ± SD, $n = 3$. $^*P < 0.05$, $^{**}P < 0.01$ between CMP + mExo^{NC} and CMP + mExo^{shTXN} groups.

presence of ubiquitin (K63R) (Fig. 5C). The lysine residues responsible for TXN ubiquitination have barely been reported. Thus, we conducted online ubiquitination site prediction (http://bdmpub.biocuckoo.org/prediction.php & https://www.uniprot.org/) and found that TXN may undergo ubiquitination modification at K3, K8, K21, K39, K61, K62, K65, and K74 sites. Then, the corresponding lysine residue was substituted with arginine. We found that TXN-K61R lost the ability to be polyubiquitinated by AMFR (Fig. 5D), thereby indicating that lysine 61 was responsible for TXN polyubiquitination mediated by TXN.

To further confirm that the polyubiquitination of TXN mediated by AMFR determined the transportation of TXN into mExo, we transfected BMSCs with MYC-tagged TXN, HA-tagged ubiquitin, and Flag-tagged AMFR plasmids and their mutants. We found that AMFR-ΔRING and TXN-K61R mutants both decreased the content of TXN in mExo (Fig. 5E) and the affinity of TXN to ESCRT proteins (Fig. 5F). Therefore, we confirmed that AMFR-mediated TXN K63-polyubiquitination at lysine 61, and AMFR-mediated TXN ubiquitination determined the affinity of TXN to ESCRT proteins and promoted the transportation of TXN into mExo.

3.5. *Downregulating AMFR impairs the protective effects of mExo against NPSC senescence*

We collected the mExo derived from BMSCs that were infected by *shAMFR* lentivirus (Supporting Information Fig. S6). Then, we evaluated whether AMFR mediated the effects of mExo against cell senescence. Within expectation, we found that the SA-β-gal positive staining rate was elevated in the mExo^{shAMFR} group compared with that in the mExo and mExo^{NC} groups (Fig. 6A and B). Moreover, the protein expression of p16 and p21 was significantly increased in the mExo^{shAMFR} group, which suggests impaired inhibitory effects on cell senescent phenotype (Fig. 6C). Cell cycle arrest was also more obvious in the mExo^{shAMFR} group as evidenced by a decreased proportion of G2/M cells (Fig. 6D).

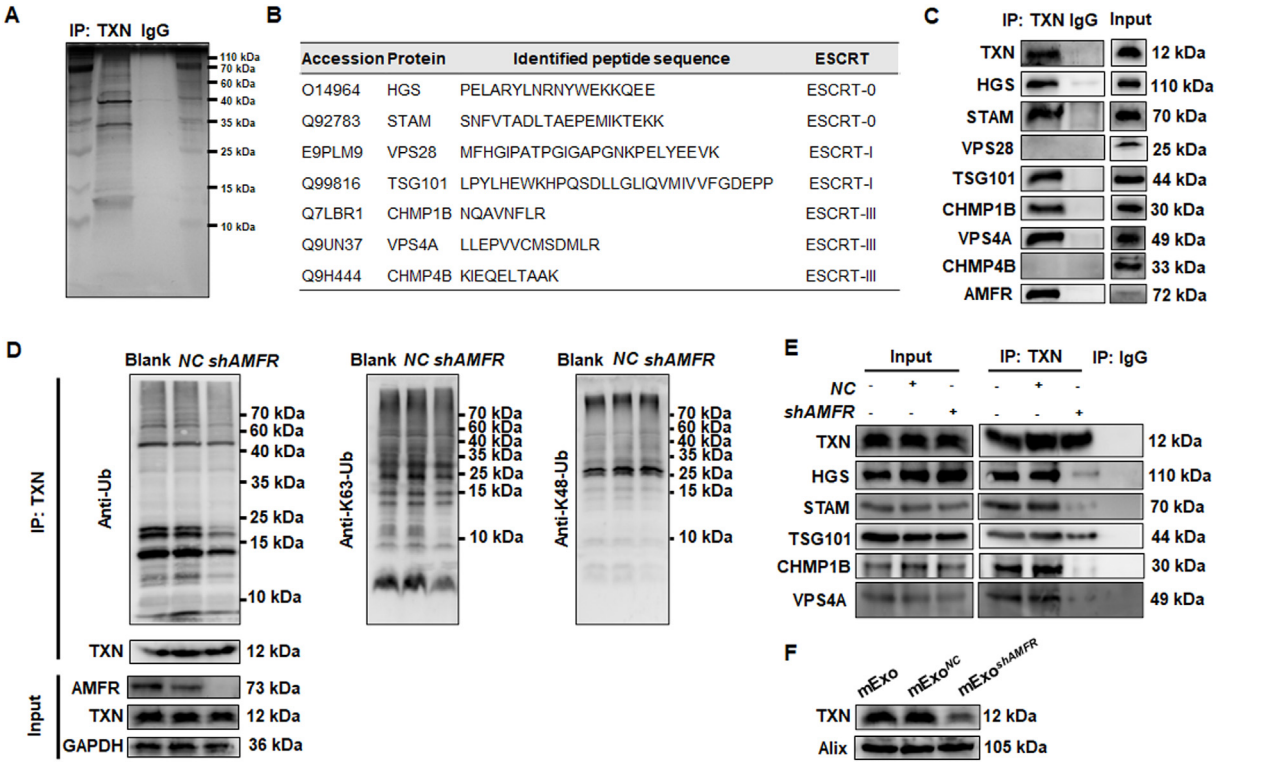

Figure 4 AMFR mediates TXN polyubiquitination and promotes the sorting of TXN into the mExo. (A) SDS-PAGE imaging of TXN immunoprecipitation. (B) Mass spectrum analysis and screening of ESCRTs binding to TXN. (C) Immunoprecipitation evaluating the binding affinity of TXN to ESCRTs and AMFR. (D) Immunoprecipitation detecting the TXN polyubiquitination in BMSCs infected by *shAMFR* lentivirus. (E) The assessment of binding affinity of TXN to ESCRTs immunoprecipitation. (F) Western blot analysis of TXN content in mExo derived from BMSCs treated with *shAMFR* lentivirus.

Therefore, AMFR knock-down in BMSCs impairs the protective effects of mExo against NPSCs senescence.

3.6. *Exosomal TXN regulates the transcriptional activity of NRF2 to establish an anti-oxidative pattern*

We used RNA sequencing to analyze gene expression profiling of NPSCs exposed to mExo or mExo^{shTXN} under 1.0 MPa compression for 36 h to investigate the mechanisms underlying the effect of exosomal TXN on NPSCs. Gene set enrichment analysis (GSEA) for several predefined gene lists (negative regulation of cellular senescence [GO:2000773], oxidative stress induced senescence [R-HSA-2559580], replicative senescence [GO:0090399], and senescence-associated secretory phenotype (SASP)[R-HSA-2559582]) indicated that these senescence-associated pathways were transcriptionally regulated after TXN was presented into NPSCs by mExo (Fig. 7A). To identify key transcriptional circuits regulated by exosomal TXN in NPSCs, we used the Virtual Inference of Protein Activity by Enriched Regulon analysis (VIPER) algorithm to predict transcription factor activities. The results showed that, compared with the mExo group, the transcriptive activity of NRF2 (*NFE2L2,* Nuclear factor, erythroid 2-like 2) was downregulated in the mExo^{shTXN} group (Fig. 7B). NRF2 is an endogenous antioxidant transcription factor that regulates the expression of antioxidative genes and cytoprotective enzymes to maintain intracellular redox homeostasis[26], which may mediate the anti-senescence effects of exosomal TXN. Supportively, the ChIP assay showed that exogenous TXN (10 μg/mL)[27] significantly promoted the transcriptive activity of NRF2 by promoting its affinity to its downstream gene promoters (Fig. 7C). Besides, we compared the anti-senescence effects of recombinant TXN and mExo, and the 10 μg/mL of TXN was comparable to that of 100 μg/mL mExo (Supporting Information Fig. S7). Moreover, the transcriptive activity of Nrf2 was downregulated in the mExo^{shTXN} group compared with that in the mExo group (Fig. 7D). Furthermore, the expression of NRF2 downstream genes, *CAT*, *NQO1*, and *SOD* were significantly upregulated after exogenous TXN treatment (Supporting Information Fig. S8). Then, we knock down NRF2 in NPSCs to evaluate whether NRF2 mediated the protective effects of mExo against NPSCs senescence. After NRF2 knock-down, the downregulatory effects of mExo on the SA-β-gal positive staining rate were reversed (Fig. 7E). Reactive oxygen species (ROS) accumulation in NPSCs was significantly increased when cells were exposed to 1.0 MPa compression, which was alleviated by mExo. NRF2 knock-down increased intracellular ROS accumulation (Fig. 7F). Moreover, cell cycle arrest was aggravated in the compression (CMP) + mExo + *shNRF2* group, compared with that in the CMP + mExo group (Fig. 7G). The protein expression of p16 and p21 was also increased after *NRF2* knock-down, in the presence of mExo (Fig. 7H), suggesting that NRF2 is the downstream pathway mediating the anti-senescence effects of mExo.

3.7. *The composite NRF2/AP-1 pathway forms a feed-forward circuit to maintain the production of TXN in NPSCs*

TXN has also been reported to be critical in the AP-1 transcriptive activity[28]. Besides, JUN stimulates the transcription of NRF2.

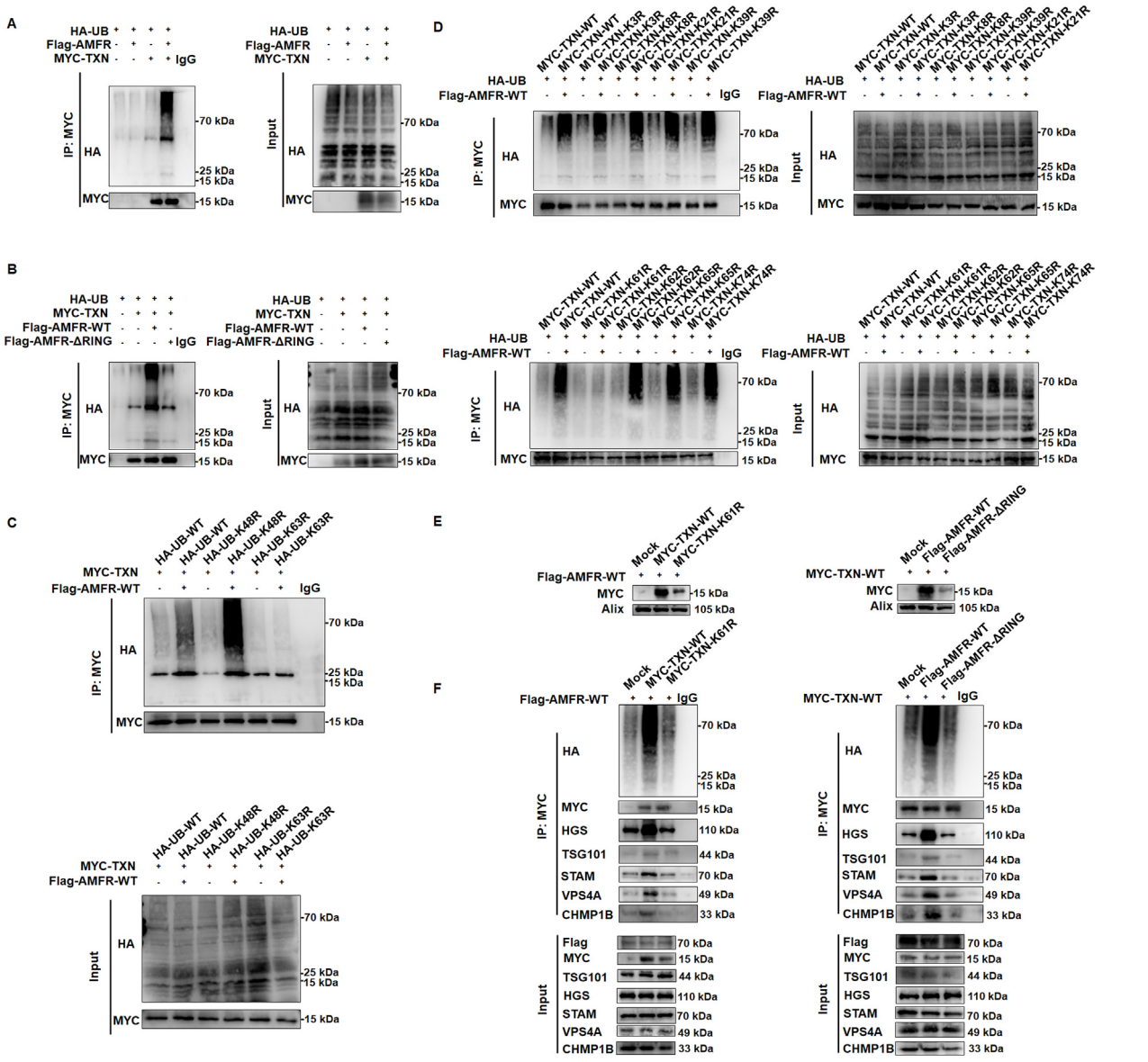

Figure 5 AMFR catalyzes TXN polyubiquitination and determines its transportation into mExo. (A) Co-IP analysis of TXN ubiquitination in HEK293T cells transfected with plasmids encoding MYC-TXN, HA-ubiquitin, and Flag-AMFR. (B) Co-IP analysis of TXN ubiquitination in HEK293T cells transfected with plasmids encoding MYC-TXN and HA-ubiquitin, as well as Flag-AMFR-WT or Flag-AMFR-ΔRING. (C) Co-IP analysis of TXN ubiquitination in HEK293T cells transfected with plasmids encoding MYC-TXN and Flag-AMFR, a control vector or plasmids encoding HA-ubiquitin (K48R) or HA-ubiquitin (K63R). (D) Co-IP analysis of TXN ubiquitination in HEK 293T cells transfected with plasmids encoding HA-ubiquitin, Flag-AMFR, and MYC-TXN or its mutant. (E) Protein content of TXN in mExo derived from BMSCs transfected with MYC-TXN and Flag-AMFR or their mutants. (F) Co-IP analysis detecting the affinity of TXN to ESCRT proteins in BMSCs transfected with MYC-TXN and Flag-AMFR or their mutants.

Therefore, we were curious whether there was a regulatory circuit among these proteins[29]. We found that mExo promoted the nuclear expression of c-FOS and c-JUN, which was inhibited by knocking down exosomal TXN (Fig. 8A). Besides, mExo promoted the binding of c-FOS, c-JUN, and JUNB to the AP-1-binding motif, TPA-responsive element (TRE) (5′-TGAGTCA-3′). The application of an AP-1 activity inhibitor and knocking down exosomal TXN reduced the binding of AP-1-related proteins to TRE (Fig. 8B), indicating that exosomal TXN mediated the inductive effects of AP-1 activity of mExo. Besides, exogenous TXN increased the binding of AP-1-related proteins to TRE (Supporting Information Fig. S9). ChIP assay indicated that T-5224 decreased the binding affinity of NRF2 to its downstream genes' promoters (Fig. 8C). TXN pathway is a downstream component of NRF2-regulated anti-oxidative system[30]. We found that knocking down NRF2 reduced the protein content of TXN in NPSCs in the presence of mExo (Fig. 8D), while the TXN content in mExo was not altered by *shNRF2* (Supporting Information Fig. S10). Besides, the NRF2 agonists promoted the accumulation of TXN in NPSCs and restored the anti-senescence effects of mExo^{shTXN} (Supporting Information Fig. S11). The inhibition of AP-1 and exosomal TXN both reversed the promotive effects of mExo on the protein

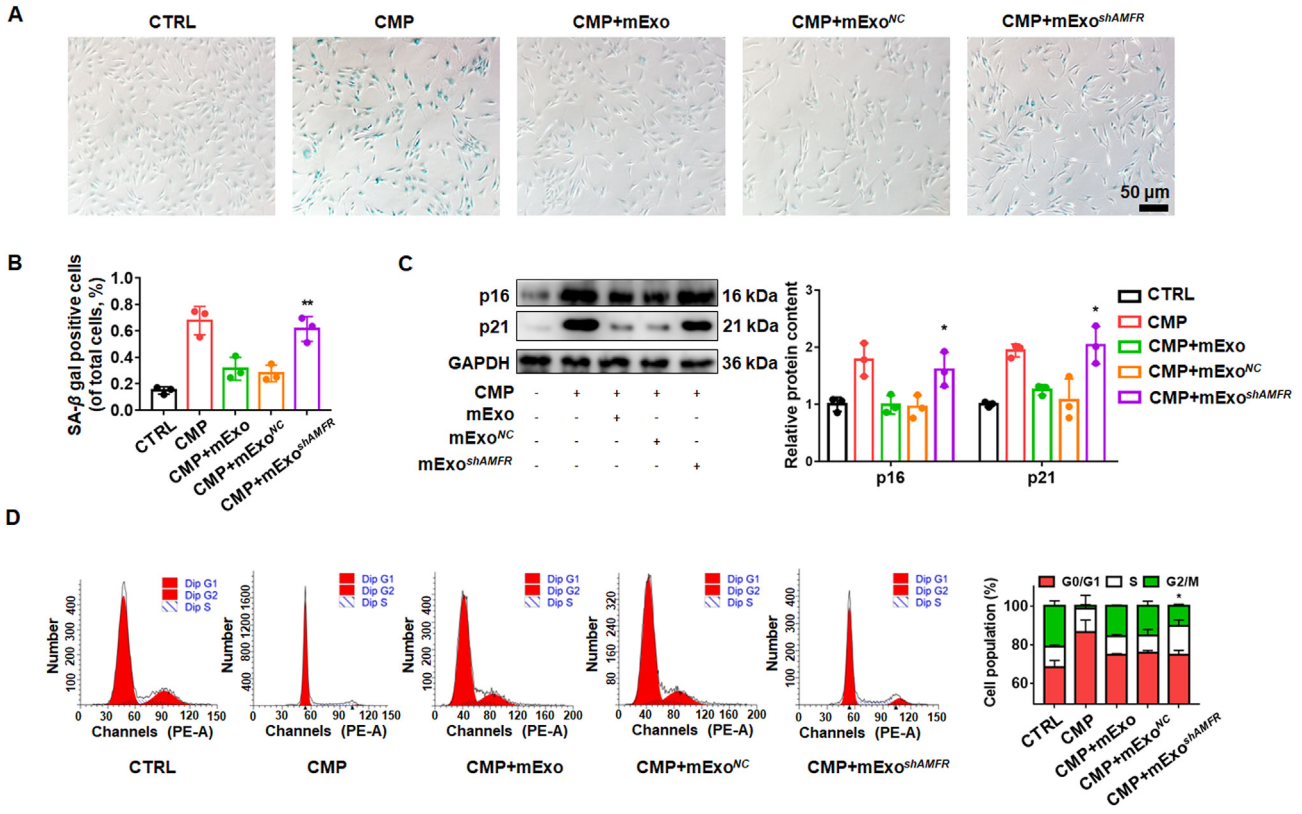

Figure 6 AMFR mediated the protective effects of mExo against NPSCs senescence. (A) SA-β-gal staining of NPSCs treated with compression and mExo. (B) Quantitative analysis of the percentage of SA-β-gal positive staining cells. Scale bar, 50 μm. (C) Western blot and densitometric analysis of p16 and p21 expression in NPSCs with different treatments. Densitometric analysis was normalized to the CTRL group. (D) Flow cytometry showing the distribution of the cells in G0/G1, S, and G2/M phases. Data are presented as the mean ± SD, $n = 3$. $^*P < 0.05$, $^{**}P < 0.01$ between CMP + mExo^{NC} and CMP + mExo^{shAMFR} groups.

content of TXN in NPSCs (Fig. 8E−G and Supporting Information Fig. S12). Then, we detected the *TXN* mRNA expression level to evaluate whether mExo promotes the endogenous transcription of *TXN* in NPSCs. RT-qPCR analysis confirmed that mExo increased the *TXN* mRNA expression in NPSCs, which was reduced by knocking down exosomal TXN, cellular NRF2, or the inhibition of AP-1 activity (Fig. 8H). Therefore, exosomal TXN regulated the activity of NRF2 and AP-1 which control the expression of TXN in NPSCs, thereby forming a feed-forward loop to promote the accumulation of TXN in NPSCs (Fig. 8I).

3.8. Exosomal TXN/NRF2 pathway mediates the protective effects of mExo against IDD

To evaluate the role of exosomal TXN and NRF2 *in vivo*, we injected mExo, mExo^{NC}, mExo^{shTXN}, *NC vehicle*, or adenovirus-*shNRF2* into discs at 7th days after the establishment of rat IDD model. After 4 weeks, T2-weighted MRI and histological examinations were conducted to assess the severity of IDD. The immunofluorescent assay confirmed the *in vivo* knockdown efficiency of adenovirus-*shNRF2* (Supporting Information Fig. S13). MRI images showed that the T2WI intensity in the IDD group was lower than that in the intact group, while mExo rescued the loss of T2WI intensity (Fig. 9A). Knocking down exosomal TXN or NRF2 caused the downregulation of T2WI intensity and decreased water content (Fig. 9A). Modified Pfirmann grading[31] showed that the degenerative grade was significantly increased after exosomal TXN or NRF2 knock-down (Fig. 9A). HE and SO staining were applied to evaluate the histological changes. IDD group showed ruptured or serpentine fibers in annulus fibrosus, a severe decrease of cell clusters, and crumpled nucleus pulposus shape, and mExo improved the morphology of degenerated discs, which was reversed by knocking down exosomal TXN or NRF2 (Fig. 9B). mExo reduced intradiscal accumulation of ROS in the IDD model, while IDD + mExo^{shTXN} and IDD + mExo^{NC} + *shNRF2* group showed significantly increased ROS accumulation (Fig. 9C). Besides, we found that the expression of p16 and p21 in TEK$^+$ cells significantly decreased in the mExo group, while knocking down exosomal TXN or NRF2 upregulated the expression of these senescence-related proteins in TEK$^+$ cells (Supporting Information Fig. S14). Therefore, the protective effects of mExo against IDD were regulated by exosomal TXN and NRF2.

4. Discussion

As a promising cell-free strategy for IDD therapy, the application of mExo in the treatment of IDD has been broadly investigated[32]. mExo serves as an alternative for stem cell therapy to overcome its shortage, including impaired cell viability in harsh IDD microenvironment, aggravation of nutrient deficiency, and limited tissue penetration[33]. The mechanisms of mExo on inhibiting IDD inflammation, and regulating mature nucleus pulposus cells apoptosis and proliferation have been partially illustrated. We spotted that the ability of proliferation and differentiation of

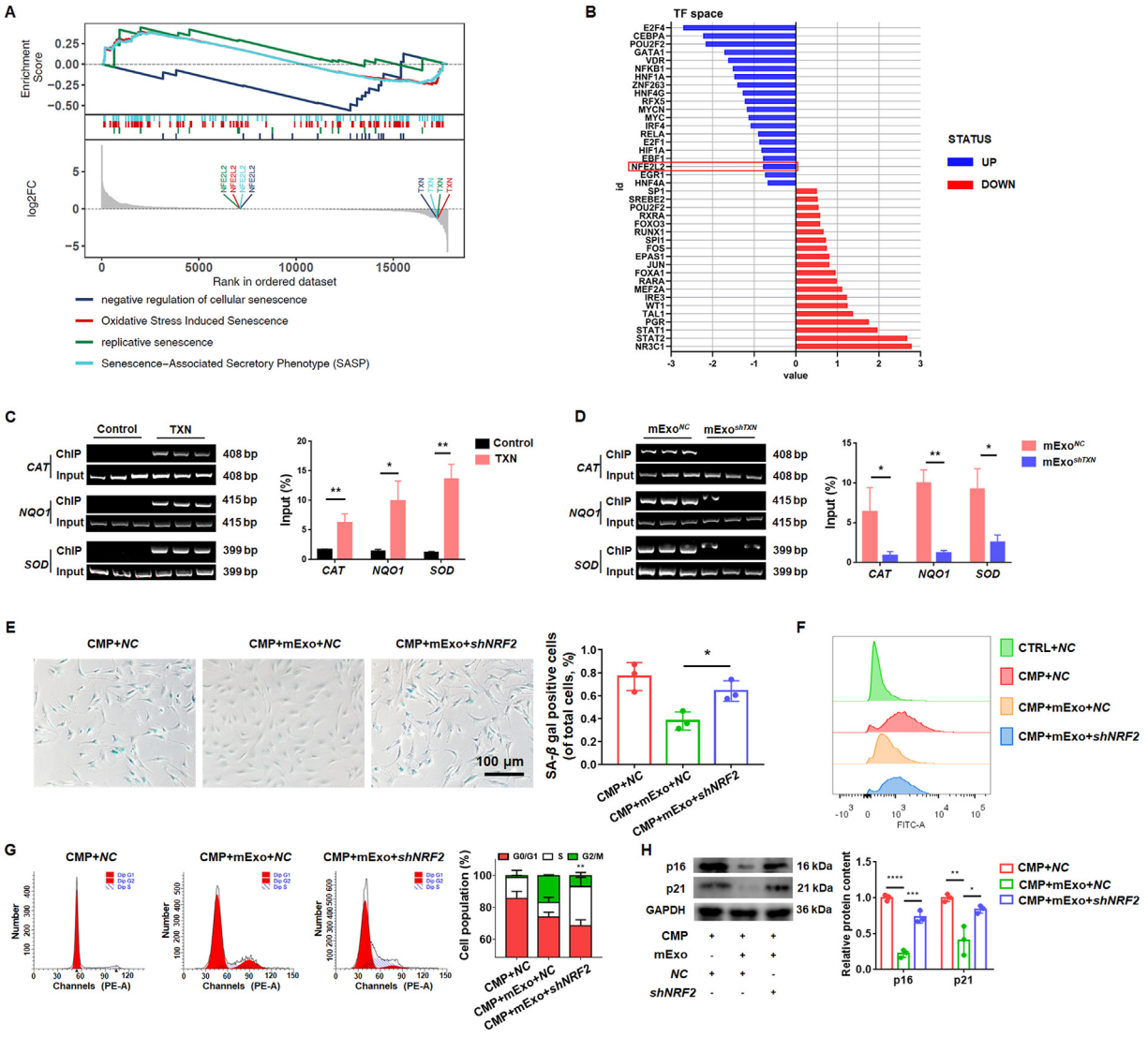

Figure 7 Exosomal TXN alleviates compression-induced NPSCs senescence by regulating NRF2 transcriptive activity. (A) Gene set enrichment analysis (GSEA) of the fold change-ranked gene list showed that exosomal TXN regulated the normalized enrichment scores for each predefined senescence-associated gene sets. The gene names *TXN* and *NFE2L2* (NRF2) in the ranked list part and all genes in the metric part were colored as same as their correlated pathways. (B) Prediction of transcription factor activities showed that the transcriptive activity of NRF2 was downregulated in the mExo^{shTXN} group. (C) ChIP assay suggested that exogenous TXN promoted the binding affinity of NRF2 to *CAT*, *NQO1*, and *SOD* promoters. (D) ChIP assay showed that exosomal TXN knock-down inhibited NRF2 binding to *CAT*, *NQO1*, and *SOD* promoters. ChIP data were normalized to input. (E) *NRF2* knock-down increased the percentage of SA-β-gal positive staining cells. Scale bar, 100 μm. (F) DCFH-DA assay showed increased accumulation of intercellular ROS in NPSCs with *NRF2* knock-down. (G) Decreased proportion of G2/M cells was identified after *NRF2* knock-down. (H) Western blot analysis showed upregulated expression of p16 and p21 in NPSCs with *NRF2* knock-down. Densitometric analysis was normalized to the CMP group. Data are presented as the mean ± SD, $n = 3$. $^*P < 0.05$, $^{**}P < 0.01$, $^{***}P < 0.001$, $^{****}P < 0.0001$ between groups.

senescent NPSCs was reduced, resulting in the failure of endogenous repair[9,10]. How mExo influences the bioactivity of NPSCs and modifies their endogenous repair capacity has not been clarified[18]. In this study, we identified that TXN mediated the protective role of mExo against NPSCs senescence, and clarified that AMFR-mediated TXN ubiquitination promoted the sorting of TXN into MSC-mExo. After being transported into NPSCs, exosomal TXN promoted endogenous TXN production *via* the TXN/NRF2/AP-1 feed-forward circuit. To our knowledge, this is the first report that explains the intercellular transport of TXN, and its related feed-forward circuit in mExo-mediated IDD regeneration.

TXN, with a conserved active-site sequence (Cys Gly Pro Cys), contains two cysteines (dithiol) that can undergo reversible redox change between an oxidized disulfides (−S−S−) and a reduced dithiol (−SH, −SH)[34]. By coupling with peroxidases or peroxiredoxins, TXN quenches oxygen species and maintains redox homeostasis[34]. Therefore, TXN participates in various kinds of processes that are related to redox changes, including gene expression, cell death, signal transduction, etc. Overexpression of TXN in mice increased the resistance of proteins and lipids to oxidative stress, and reduced the oxidative damage, thereby resulting in a prolonged life span[35,36]. In our study, we intersected the mExo

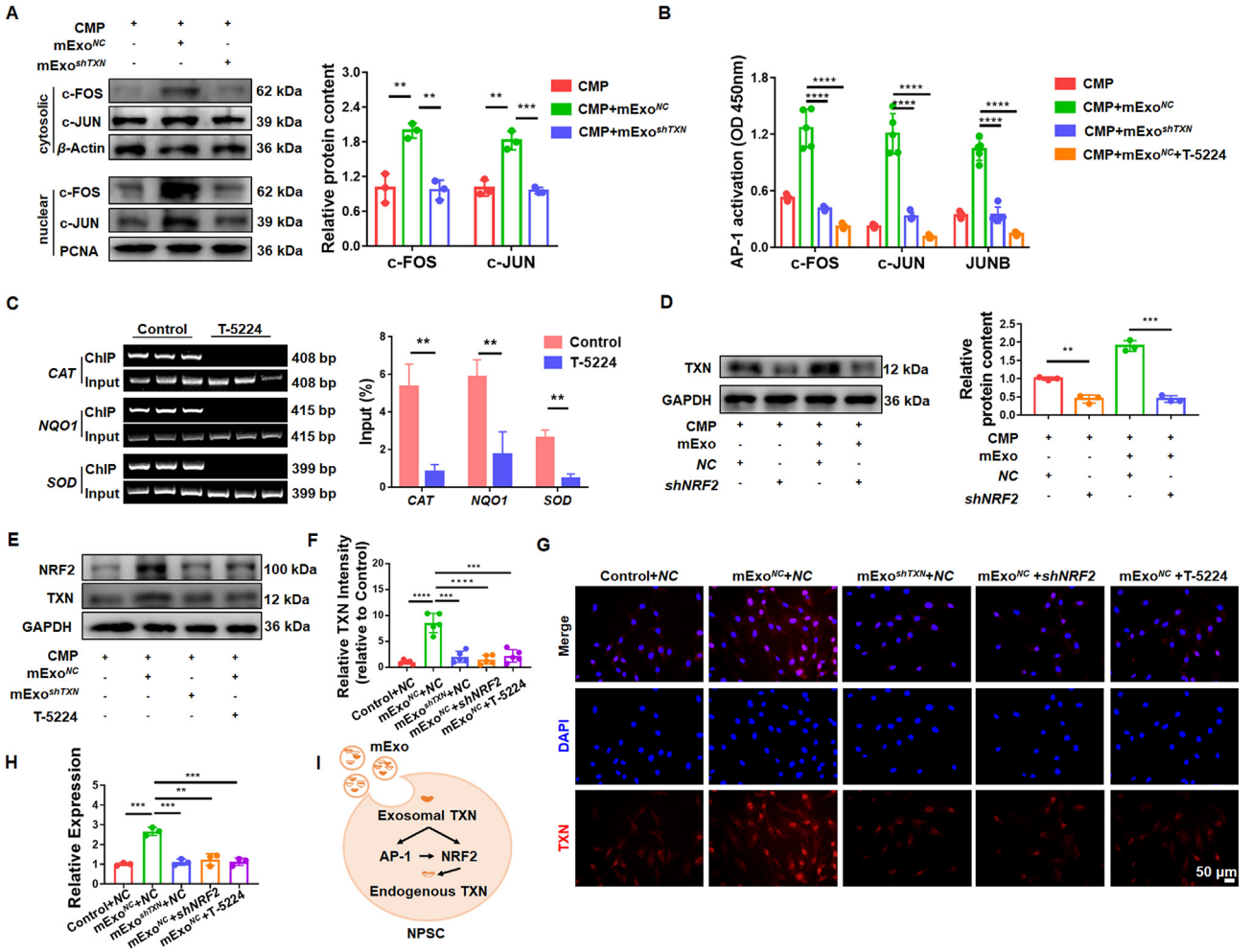

Figure 8 NRF2/AP-1 pathway forms a feed-forward circuit to promote TXN production in NPSCs. (A) Western blot analysis indicated an increased nuclear expression of c-FOS and c-JUN in NPSCs treated with mExo and a downregulated expression after knocking down exosomal TXN. (B) AP-1 binding assay suggested that inhibition of exosomal TXN and AP-1 activity reduced the binding activity of c-FOS, c-JUN, and JUNB on the TRE motif. Data are presented as the mean ± SD, $n = 5$. (C) ChIP assay showed a decreased binding affinity of NRF2 to *CAT*, *NQO1*, and *SOD* promoters when AP-1 activity was inhibited. ChIP data were normalized to input. Data are presented as the mean ± SD, $n = 3$. (D) TXN protein expression in NPSCs was downregulated by NRF2 knock-down. (E) Western blot analysis showed that NRF2 and TXN expression was reduced after inhibition of exosomal TXN and AP-1 activity. Densitometric analysis of Western blot was normalized to the control group. Data are presented as the mean ± SD, $n = 3$. (F) Quantitative data analyzed the TXN intensity in NPSCs normalized to the control group. Data are presented as the mean ± SD, $n = 5$. (G) Representative fluorescence images illustrated the production of TXN in NPSCs with different treatments. (H) RT-qPCR confirmed that the *TXN* mRNA expression was downregulated by knocking down *NRF2* or exosomal TXN or T-5224. Data are presented as the mean ± SD, $n = 3$. (I) Diagram illustrates that mExo transports exosomal TXN to activate AP-1 and NRF2, forming a feed-forward loop to promote the accumulation of TXN in NPSCs. $^*P < 0.05$, $^{**}P < 0.01$, $^{***}P < 0.001$, $^{****}P < 0.0001$ between groups.

proteins with senescence-related genes in the GSEA database and obtained a gene set containing TXN. Since TXN is greatly associated with redox modification and aging, we suspected that TXN mediated the anti-senescence effects of mExo. Besides, the treatment of the NPSCs with 100 μg/mL mExo resulted in a lower amount of TXN but showed comparable anti-senescence effects to the 10 μg/mL TXN treatment group, which suggests that mExo might exert anti-senescence effects *via* increasing the bioavailability of TXN. Supportively, the results indicate that after knocking down TXN in mExo, the effects of mExo on delaying NPSC senescence were significantly inhibited. Therefore, TXN is transported into NPSCs *via* mExo to exhibit the anti-senescence effects.

Then, we were curious about the mechanism of TXN secretion. It is believed that TXN is secreted by unconventional protein secretion pathways for lack of N-terminal signal sequence[37]. Whereas, the specific mechanism of TXN secretion remained a mystery[38,39]. Generally, proteins and other molecules are selectively incorporated into intraluminal vesicles (ILVs) within multivesicular regions of endosomes to be exported by mExo[40]. Then, ILVs are transported toward late endosomes and lysosomes to degrade the cargoes, or secreted into the extracellular milieu to form mExo, which transports cargos for intercellular communication[41,42]. The ESCRT system is the best-understood pathway for the incorporation of cargo into ILVs[43]. ESCRTs are characterized into ESCRT-0, ESCRT-I, ESCRT-II, and ESCRT-III. ESCRT-0, ESCRT-I, and ESCRT-II contain ubiquitin-binding and membrane-binding domains to recognize and retain ubiquitylated cargoes at endosomal membranes, sorting the proteins into ILVs[44]. ESCRT-III is unable to sort proteins for the lack of

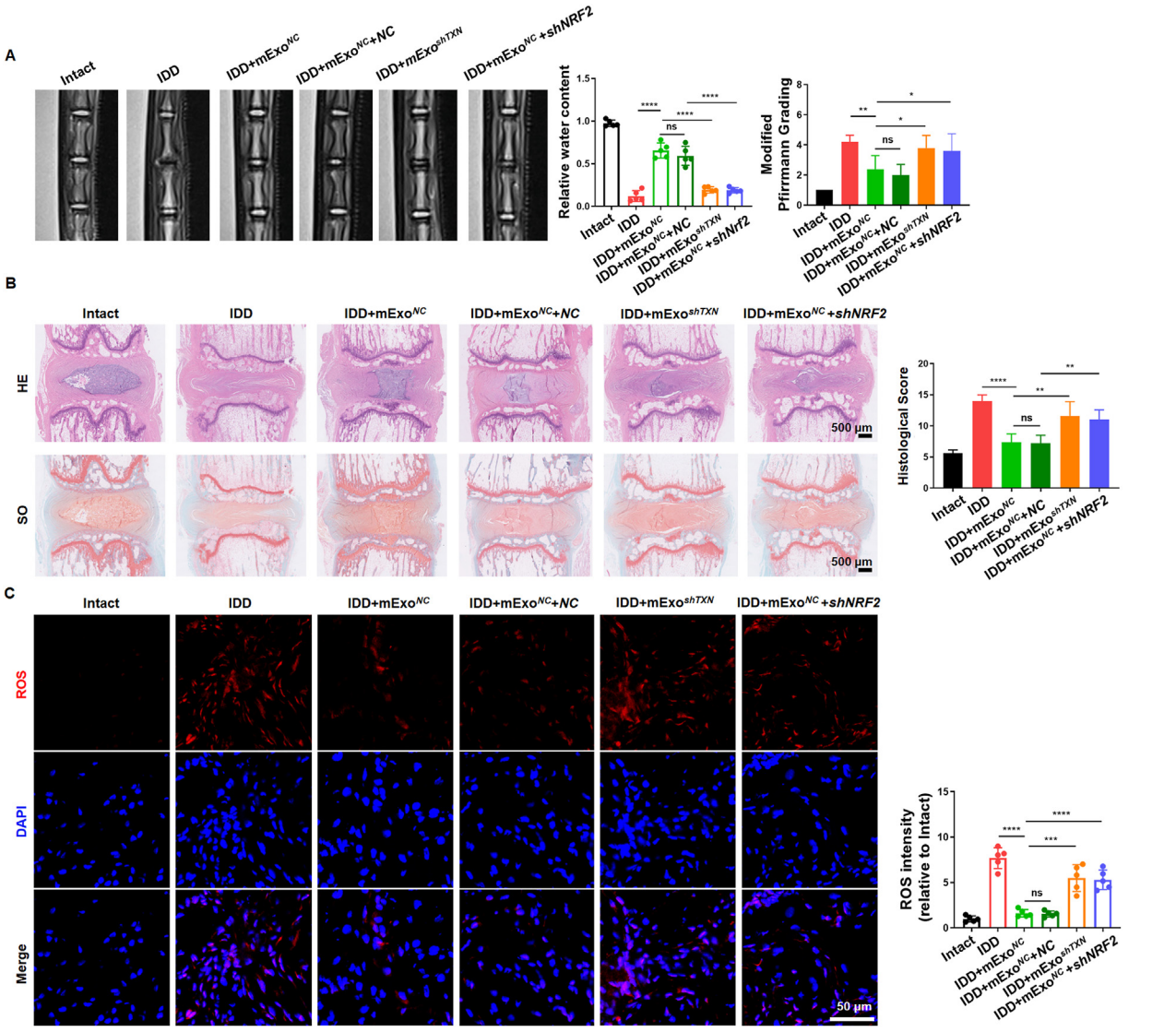

Figure 9 Exosomal TXN/NRF2 pathway regulates the promotive effects of mExo on disc regeneration. (A) Representative T2-weighted MRI images of rat caudal vertebrae. The degenerative grades according to Pfirrmann Grade and quantitative analysis of water content of operated discs based on T2WI images. (B) Representative HE and SO staining of IDD discs and the degenerative grades based on histological images. (C) Representative fluorescence images and quantification analysis evaluating the intradiscal ROS accumulation in each treatment group of disc tissues. Data are presented as the mean ± SD, $n = 3$. $^{*}P < 0.05$; $^{**}P < 0.01$; $^{***}P < 0.001$; $^{****}P < 0.0001$.

ubiquitin recognition subunits, but recruits de-ubiquitinase to remove the ubiquitinated tags on proteins in ILVs and promotes the budding of ILVs[25]. Co-IP and LC−MS results indicated that TXN bound to various kinds of ESCRTs, which shows that TXN was sorted into mExo by ESCRT pathway. Besides, TXN can be modified by ubiquitination, and AMFR serves as an E3 ubiquitin ligase for TXN ubiquitination[45]. AMFR, also known as Glycoprotein 78, participates in various cellular pathways including innate immune response, mitophagy, glucose metabolism, etc., *via* its E3 ubiquitin ligase activity[46]. Supportively, we validated that TXN was a substrate of AMFR, and firstly identified that AMFR promoted TXN K63 ubiquitination on lysine 61, which facilitated the sorting of TXN into mExo.

To further explore the mechanism of exosomal TXN in relieving NPSCs senescence, we performed RNA sequencing and found that exosomal TXN significantly changed the transcription pattern in NPSCs, among which the transcriptional activity of NRF2 was downregulated after knocking down TXN in mExo. NRF2, a master endogenous antioxidant transcription factor, controls the expression of various antioxidative genes and cytoprotective enzymes that maintain intracellular redox homeostasis[47]. Therefore, TXN may mediate the redox homeostasis not only by the reversible redox change of its catalytically active dithiol site but also by altering the transcription profile of NRF2. Supportively, we found that the transcriptional activity of NRF2 was significantly enhanced after exogenous TXN stimulation. However, the mechanism of exosomal TXN-regulated NRF2 transcriptional activity in NPSCs remains to be clarified.

TXN has long been known as a critical factor in the activation of AP-1 transcription factor[48−50]. TXN extracted from irradiated cells could activate AP-1 DNA binding activity in nonirradiated nuclear extracts, in the presence of redox factor 1 (REF-1)[51]. JUN, a critical component of AP-1, controls the expression of NRF2, while the regulatory effect of JUN on NRF2 is not consistent among studies[29,52]. In murine MEF K-RasG12D cells, JUN

promoted the transcription of the NRF2/*NFE2L2*[29]. However in oxidative stress-treated HeLa cells, JUN knockdown reinforces the expression of *NRF2*-related genes[52]. Thus, the transcriptive pattern of AP-1 on NRF2 may differ in different cells under different stimulation[52,53]. In our study, we proved that exosomal TXN promoted the DNA-binding activity of AP-1. AP-1 inhibition reduced the expression of NRF2 and its transcriptional activity. Therefore, exosomal TXN regulated the transcriptional activity of NRF2 in NPSCs mainly *via* AP-1.

Interestingly, TXN has been reported to be a target of NRF2 in an antioxidant response element binding manner[30,47]. We found that the knockdown of NRF2 in mExo-treated NPSCs down-regulated the expression of TXN, indicating that the production of TXN in NPSCs is regulated by NRF2. Moreover, the exosomal TXN further promoted the production of TXN in NPSCs, by the evidence of increased expression of endogenous TXN. As exosomal TXN regulated NRF2 transcriptional activity *via* AP-1, and TXN is an NRF2 target in return, TXN/NRF2/AP-1 forms a feed-forward circuit to promote the endogenous production of TXN in NPSCs. The regulatory feed-forward loops have been reported in many pathophysiological processes, including tumor progression, allodynia, thermogenesis, etc.[54−57]. Feed-forward loops usually work as maintaining a steady state of signaling activation and amplifying the signal when fast cellular reactions are required[58]. Therefore, the positive feed-forward loop of TXN/NRF2/AP-1 exerts accelerative effects on the production of TXN in NPSCs, leading to redox homeostasis and reduced cell senescence.

5. Conclusions

This work provides insight into the critical role of exosomal TXN in regulating NPSCs senescence and promoting IVD regeneration. AMFR-mediated polyubiquitination induced TXN secretion *via* ESCRT pathway by mExo. After being transported into NPSCs, exosomal TXN modified the endogenous TXN production *via* the TXN/NRF2/AP-1 feed-forward circuit. This study provides a theoretical basis for the application of mExo and elucidates the mechanisms of TXN sorting into mExo and the anti-senescence of TXN, thus, laying a solid foundation for the precise construction of anti-senescence mExo.

Acknowledgements

This study was supported by the National Natural Science Foundation of China (82202764 and 81974352), the China Postdoctoral Science Foundation (2021M701331), Natural Science Foundation of Hubei Province (2020CFB778, China), and the Scientific Research Training Program for Young Talents from Union Hospital, Tongji Medical College, Huazhong University of Science and Technology, Wuhan, China.

Author contributions

Xuanzuo Chen: Writing − original draft, Software, Methodology, Investigation, Formal analysis, Data curation, Conceptualization. Sheng Liu: Writing − original draft, Software, Methodology. Huiwen Wang: Writing − original draft, Formal analysis. Yiran Liu: Data curation, Writing − review & editing. Yan Xiao: Software. Kanglu Li: Software, Formal analysis. Feifei Ni: Data curation, Writing − review & editing. Wei Wu: Methodology. Hui Lin: Data curation. Xiangcheng Qing: Writing − review & editing, Supervision. Feifei Pu: Writing − review & editing, Supervision. Baichuan Wang: Writing − review & editing, Supervision, Funding acquisition. Zengwu Shao: Writing − review & editing, Supervision, Funding acquisition. Yizhong Peng: Writing − review & editing, Supervision, Funding acquisition, Conceptualization.

Conflicts of interest

The authors declare no conflicts of interest.

Appendix A. Supporting information

Supporting information to this article can be found online at https://doi.org/10.1016/j.apsb.2024.12.013.

References

1. Knezevic NN, Candido KD, Vlaeyen JWS, Van Zundert J, Cohen SP. Low back pain. *Lancet* 2021;**398**:78−92.
2. Cheung KMC, Samartzis D, Karppinen J, Luk KDK. Are "patterns" of lumbar disc degeneration associated with low back pain?: new insights based on skipped level disc pathology. *Spine (Phila Pa 1976)* 2012;**37**:E430−8.
3. Kamali A, Ziadlou R, Lang G, Pfannkuche J, Cui S, Li Z, et al. Small molecule-based treatment approaches for intervertebral disc degeneration: current options and future directions. *Theranostics* 2020;**11**:27−47.
4. Peng Y, Qing X, Shu H, Tian S, Yang W, Chen S, et al. Proper animal experimental designs for preclinical research of biomaterials for intervertebral disc regeneration. *Biomater Translational* 2021;**2**:91−142.
5. He R, Wang Z, Cui M, Liu S, Wu W, Chen M, et al. HIF1A alleviates compression-induced apoptosis of nucleus pulposus derived stem cells *via* upregulating autophagy. *Autophagy* 2021;**17**:3338−60.
6. Sakai D, Andersson GBJ. Stem cell therapy for intervertebral disc regeneration: obstacles and solutions. *Nat Rev Rheumatol* 2015;**11**:243−56.
7. Gao B, Jiang B, Xing W, Xie Z, Luo Z, Zou W. Discovery and application of postnatal nucleus pulposus progenitors essential for intervertebral disc homeostasis and degeneration. *Adv Sci (Weinh)* 2022:e2104888.
8. Huang D, Peng Y, Ma K, Qing X, Deng X, Li Z, et al. Puerarin relieved compression-induced apoptosis and mitochondrial dysfunction in human nucleus pulposus mesenchymal stem cells *via* the PI3K/Akt pathway. *Stem Cell Int* 2020;**2020**:7126914.
9. Liang H, Chen S, Huang D, Deng X, Ma K, Shao Z. Effect of compression loading on human nucleus pulposus-derived mesenchymal stem cells. *Stem Cell Int* 2018;**2018**:1481243.
10. Wu H, Shang Y, Yu J, Zeng X, Lin J, Tu M, et al. Regenerative potential of human nucleus pulposus resident stem/progenitor cells declines with ageing and intervertebral disc degeneration. *Int J Mol Med* 2018;**42**:2193−202.
11. Wang F, Li Z, Chen L, Yang T, Liang B, Zhang Z, et al. Inhibition of ASCT2 induces hepatic stellate cell senescence with modified proinflammatory secretome through an IL-1α/NF-κB feedback pathway to inhibit liver fibrosis. *Acta Pharm Sin B* 2022;**12**:3618−38.
12. Zhang S, Liu W, Wang P, Hu B, Lv X, Chen S, et al. Activation of HSP70 impedes *tert*-butyl hydroperoxide (t-BHP)-induced apoptosis and senescence of human nucleus pulposus stem cells *via* inhibiting the JNK/c-Jun pathway. *Mol Cell Biochem* 2021;**476**:1979−94.
13. Wang J, Xia D, Lin Y, Xu W, Wu Y, Chen J, et al. Oxidative stress-induced circKIF18A downregulation impairs MCM7-mediated anti-senescence in intervertebral disc degeneration. *Exp Mol Med* 2022;**54**:285−97.
14. Huang D, Peng Y, Li Z, Chen S, Deng X, Shao Z, et al. Compression-induced senescence of nucleus pulposus cells by promoting mitophagy activation *via* the PINK1/PARKIN pathway. *J Cell Mol Med* 2020;**24**:5850−64.

15. Rao S, He Z, Wang Z, Yin H, Hu X, Tan Y, et al. Extracellular vesicles from human urine-derived stem cells delay aging through the transfer of PLAU and TIMP1. *Acta Pharm Sin B* 2024;**14**:1166−86.
16. Liu S, Wu X, Chandra S, Lyon C, Ning B, jiang L, et al. Extracellular vesicles: emerging tools as therapeutic agent carriers. *Acta Pharm Sin B* 2022;**12**:3822−42.
17. Neupane YR, Handral HK, Alkaff SA, Chng WH, Venkatesan G, Huang C, et al. Cell-derived nanovesicles from mesenchymal stem cells as extracellular vesicle-mimetics in wound healing. *Acta Pharm Sin B* 2023;**13**:1887−902.
18. Widjaja G, Jalil AT, Budi HS, Abdelbasset WK, Efendi S, Suksatan W, et al. Mesenchymal stromal/stem cells and their exosomes application in the treatment of intervertebral disc disease: a promising frontier. *Int Immunopharmacol* 2022;**105**:108537.
19. Han B, Zhu K, Li FC, Xiao YX, Feng J, Shi ZL, et al. A simple disc degeneration model induced by percutaneous needle puncture in the rat tail. *Spine (Phila Pa 1976)* 2008;**33**:1925−34.
20. Alvarez MJ, Shen Y, Giorgi FM, Lachmann A, Ding BB, Ye BH, et al. Functional characterization of somatic mutations in cancer using network-based inference of protein activity. *Nat Genet* 2016;**48**:838−47.
21. Garcia-Martin R, Wang G, Brandão BB, Zanotto TM, Shah S, Kumar Patel S, et al. microRNA sequence codes for small extracellular vesicle release and cellular retention. *Nature* 2022;**601**:446−51.
22. Sakai D, Nakamura Y, Nakai T, Mishima T, Kato S, Grad S, et al. Exhaustion of nucleus pulposus progenitor cells with ageing and degeneration of the intervertebral disc. *Nat Commun* 2012;**3**:1264.
23. Shelar SB, Kaminska KK, Reddy SA, Kumar D, Tan CT, Yu VC, et al. Thioredoxin-dependent regulation of AIF-mediated DNA damage. *Free Radic Biol Med* 2015;**87**:125−36.
24. Cao X, He W, Pang Y, Cao Y, Qin A. Redox-dependent and independent effects of thioredoxin interacting protein. *Biol Chem* 2020;**401**:1215−31.
25. Juan T, Fürthauer M. Biogenesis and function of ESCRT-dependent extracellular vesicles. *Semin Cell Dev Biol* 2018;**74**:66−77.
26. Maldonado E, Rojas DA, Urbina F, Solari A. The use of antioxidants as potential co-adjuvants to treat chronic chagas disease. *Antioxidants (Basel)* 2021;**10**:1022.
27. Sundaramoorthy P, Wang Q, Zheng Z, Jiao Y, Chen BJ, Doan PL, et al. Thioredoxin mitigates radiation-induced hematopoietic stem cell injury in mice. *Stem Cell Res Ther* 2017;**8**:263.
28. Hirota K, Matsui M, Iwata S, Nishiyama A, Mori K, Yodoi J. AP-1 transcriptional activity is regulated by a direct association between thioredoxin and Ref-1. *Proc Natl Acad Sci U S A* 1997;**94**:3633−8.
29. DeNicola GM, Karreth FA, Humpton TJ, Gopinathan A, Wei C, Frese K, et al. Oncogene-induced Nrf2 transcription promotes ROS detoxification and tumorigenesis. *Nature* 2011;**475**:106−9.
30. Luo M, Shang L, Brooks MD, Jiagge E, Zhu Y, Buschhaus JM, et al. Targeting breast cancer stem cell state equilibrium through modulation of redox signaling. *Cell Metab* 2018;**28**:69−86.e6.
31. Griffith JF, Wang YXJ, Antonio GE, Choi KC, Yu A, Ahuja AT, et al. Modified Pfirrmann grading system for lumbar intervertebral disc degeneration. *Spine (Phila Pa 1976)* 2007;**32**:E708−12.
32. Liang W, Han B, Hai Y, Sun D, Yin P. Mechanism of action of mesenchymal stem cell-derived exosomes in the intervertebral disc degeneration treatment and bone repair and regeneration. *Front Cell Dev Biol* 2022;**9**:833840.
33. Hu S, Xing H, Zhang J, Zhu Z, Yin Y, Zhang N, et al. Mesenchymal stem cell-derived extracellular vesicles: immunomodulatory effects and potential applications in intervertebral disc degeneration. *Stem Cell Int* 2022;**2022**:7538025.
34. Liu Y, Xue N, Zhang B, Lv H, Li S. Role of thioredoxin-1 and its inducers in human health and diseases. *Eur J Pharmacol* 2022;**919**:174756.
35. Cunningham GM, Roman MG, Flores LC, Hubbard GB, Salmon AB, Zhang Y, et al. The paradoxical role of thioredoxin on oxidative stress and aging. *Arch Biochem Biophys* 2015;**576**:32−8.
36. Pérez VI, Cortez LA, Lew CM, Rodriguez M, Webb CR, Van Remmen H, et al. Thioredoxin 1 overexpression extends mainly the earlier part of life span in mice. *J Gerontol A Biol Sci Med Sci* 2011;**66**:1286−99.
37. Rubartelli A, Bajetto A, Allavena G, Wollman E, Sitia R. Secretion of thioredoxin by normal and neoplastic cells through a leaderless secretory pathway. *J Biol Chem* 1992;**267**:24161−4.
38. Yodoi J, Matsuo Y, Tian H, Masutani H, Inamoto T. Anti-inflammatory thioredoxin family proteins for medicare, healthcare and aging care. *Nutrients* 2017;**9**:1081.
39. Léveillard T, Aït-Ali N. Cell signaling with extracellular thioredoxin and thioredoxin-like proteins: insight into their mechanisms of action. *Oxid Med Cell Longev* 2017;**2017**:8475125.
40. Scott CC, Vacca F, Gruenberg J. Endosome maturation, transport and functions. *Semin Cell Dev Biol* 2014;**31**:2−10.
41. Kalra H, Simpson RJ, Ji H, Aikawa E, Altevogt P, Askenase P, et al. Vesiclepedia: a compendium for extracellular vesicles with continuous community annotation. *PLoS Biol* 2012;**10**:e1001450.
42. Larios J, Mercier V, Roux A, Gruenberg J. ALIX- and ESCRT-III-dependent sorting of tetraspanins to exosomes. *J Cell Biol* 2020;**219**.
43. Hurley JH, Odorizzi G. Get on the exosome bus with ALIX. *Nat Cell Biol* 2012;**14**:654−5.
44. Mosesso N, Nagel MK, Isono E. Ubiquitin recognition in endocytic trafficking—with or without ESCRT-0. *J Cell Sci* 2019;**132**:jcs232868.
45. Chu Y, Dong X, Kang Y, Liu J, Zhang T, Yang C, et al. The chaperone BAG6 regulates cellular homeostasis between autophagy and apoptosis by holding LC3B. *iScience* 2020;**23**:101708.
46. Joshi V, Upadhyay A, Kumar A, Mishra A. Gp78 E3 ubiquitin ligase: essential functions and contributions in proteostasis. *Front Cell Neurosci* 2017;**11**:259.
47. Tonelli C, Chio IIC, Tuveson DA. Transcriptional regulation by Nrf2. *Antioxid Redox Signal* 2018;**29**:1727−45.
48. Sun Y, Oberley LW. Redox regulation of transcriptional activators. *Free Radic Biol Med* 1996;**21**:335−48.
49. Abate C, Patel L, Rauscher FJ 3rd, Curran T. Redox regulation of fos and jun DNA-binding activity *in vitro*. *Science* 1990;**249**:1157−61.
50. Brandes N, Schmitt S, Jakob U. Thiol-based redox switches in eukaryotic proteins. *Antioxid Redox Signal* 2009;**11**:997−1014.
51. Wei SJ, Botero A, Hirota K, Bradbury CM, Markovina S, Laszlo A, et al. Thioredoxin nuclear translocation and interaction with redox factor-1 activates the activator protein-1 transcription factor in response to ionizing radiation. *Cancer Res* 2000;**60**:6688−95.
52. Zolotukhin PV, Belanova AA. *Feed-forward and feed-back circuits of the NRF2/AP-1 composite pathway*. 2016. Netherlands.
53. Cho HJ, Kang JH, Kwak JY, Lee TS, Lee IS, Park NG, et al. Ascofuranone suppresses PMA-mediated matrix metalloproteinase-9 gene activation through the Ras/Raf/MEK/ERK- and Ap1-dependent mechanisms. *Carcinogenesis* 2007;**28**:1104−10.
54. Qu L, Wu Z, Li Y, Xu Z, Liu B, Liu F, et al. A feed-forward loop between lncARSR and YAP activity promotes expansion of renal tumour-initiating cells. *Nat Commun* 2016;**7**:12692.
55. Rokavec M, Öner MG, Li H, Jackstadt R, Jiang L, Lodygin D, et al. IL-6R/STAT3/miR-34a feedback loop promotes EMT-mediated colorectal cancer invasion and metastasis. *J Clin Invest* 2014;**124**:1853−67.
56. Lu Y, Dong H, Gao Y, Gong Y, Ren Y, Gu N, et al. A feed-forward spinal cord glycinergic neural circuit gates mechanical allodynia. *J Clin Invest* 2013;**123**:4050−62.
57. Lin Y, Xiao L, Cai Q, Zhu C, Li S, Li B, et al. The chemerin−CMKLR1 axis limits thermogenesis by controlling a beige adipocyte/IL-33/type 2 innate immunity circuit. *Sci Immunol* 2021;**6**:eabg9698.
58. Salminen A. Feed-forward regulation between cellular senescence and immunosuppression promotes the aging process and age-related diseases. *Ageing Res Rev* 2021;**67**:101280.